CCFE-PR(13)69

S. Saarelma, M.N.A. Beurskens, D. Dickinson, L. Frassinetti,
M.J.Leyland, C.M. Roach, EFDA-JET Contributors

MHD and Gyro-kinetic Stability of JET Pedestals

MHD and Gyro-kinetic Stability of JET Pedestals

S. Saarelma[1], M.N.A. Beurskens[1], D. Dickinson[1], L. Frassinetti[3], M.J.Leyland[2], C.M. Roach[1], EFDA-JET Contributors[*]

[1]EURATOM/CCFE Fusion Association, Culham Science Centre, OX14 3DB Abingdon (UK)
[2]York Plasma Institute, Dept. of Physics, University of York, York, YO10 5DD, UK
[3]Division of Fusion Plasma Physics, School of Electrical Engineering, Royal Institute of Technology, Association EURATOM-VR, Stockholm, Sweden

The following article appeared in Nuclear Fusion, Vol.53, No.12, December 2013, p.123012

The following article appeared in Nuclear Fusion, Vol.53, No.12, December 2013, p.123012

MHD and gyro-kinetic stability of JET pedestals
Saarelma S, Beurskens M N A, Dickinson D, Frassinetti L, Leyland M J, Roach C M, EFDA-JET Contributors

MHD and Gyro-kinetic Stability of JET Pedestals

December 5, 2013

S. Saarelma†, M.N.A. Beurskens†, D. Dickinson†, L. Frassinetti§, M.J. Leyland‡, C.M. Roach†, EFDA-JET Contributors [1]
JET-EFDA, Culham Science Centre, Abingdon, OX14 3DB, UK
†Euratom/CCFE Fusion Association, Culham Science Centre, OX14 3DB, Abingdon, UK
‡York Plasma Institute, Dept. of Physics, University of York, York, YO10 5DD, UK
§Division of Fusion Plasma Physics, School of Electrical Engineering, Royal Institute of Technology, Association EURATOM-VR, Stockholm, Sweden

samuli.saarelma@ccfe.ac.uk

Abstract

The pedestal profile measurements in high triangularity JET plasmas show that with low fuelling the pedestal width decreases during the ELM cycle and with high fuelling it stays constant. In the low fuelling case the pedestal pressure gradient keeps increasing until the ELM crash and in the high fuelling case it initially increases then saturates during the ELM cycle.

Stability analysis reveals that both JET plasmas become unstable to finite-n ideal MHD peeling-ballooning modes at the end of the ELM cycle. During the ELM cycle, $n = \infty$ ideal MHD ballooning modes and kinetic

[1] See the Appendix of F. Romanelli et al., Proceedings of the 24th IAEA Fusion Energy Conference 2012, San Diego, USA

ballooning modes are found to be locally stable in most of the steep pressure gradient region of the pedestal owing to the large bootstrap current, but to be locally unstable in a narrow region of plasma at the extreme edge.

Unstable micro-tearing modes are found at the JET pedestal top, but they are sub-dominant to ion temperature gradient modes. They are insensitive to collisionality and stabilised by increasing density gradient.

1 Introduction

The global plasma confinement in a tokamak operating in high confinement or H-mode is largely determined by the edge pedestal pressure due to core turbulence restricting $\nabla T/T$ near the marginal stability limit[1]. Therefore, being able to predict the edge pedestal behaviour allows prediction of the achievable core pressure and the fusion power. There is strong evidence from various devices that in Type I ELMy H-mode the pedestal pressure is constrained by ideal MHD peeling-ballooning modes. When the stability limit is exceeded, the peeling-ballooning mode is thought to trigger an instability causing an ELM crash that reduces the pedestal top pressure. The stability calculations of JET [2], DIII-D [3], JT-60U [4] and ASDEX Upgrade [3] have all found plasma to be within error margin of the peeling-ballooning stability limit prior to a Type I ELM crash.

However, the peeling-ballooning constraint does not solely determine the pedestal pressure. By increasing the width of the pedestal it is possible to maintain peeling-ballooning stability at higher pedestal top pressure with a reduced pressure gradient. In order to uniquely predict the maximum achievable pedestal height, the pedestal width also has to be constrained. The EPED1 model uses a width scaling derived from the physics of kinetic ballooning modes, $\Delta_{ped} = 0.076\beta_{p,ped}^{0.5}$, combined with the peeling-ballooning stability limit to determine the height of the pedestal [5]. Pedestal measurements from ASDEX-Upgrade, DIII-D, and JET have been shown to be consistent with EPED1 model predictions [6]. A more advanced version of EPED, EPED 1.6, replaces the scaling law constraint with a procedure, outlined in [7], that extrapolates from local ideal MHD stability calculations for $n = \infty$ ballooning modes to approximate the stability of kinetic ballooning modes (KBM). Both the linear growth rate and the non-linear heat flux from KBMs increase very rapidly after the stability limit is exceeded, constraining the pedestal pressure gradient below this limit [8]. While the local calcula-

tion in the pedestal region may not be sufficient to solve the turbulent heat fluxes due to radial requirements of the computational box, linear analysis can provide the local stability boundary.

In recent gyrokinetic studies of MAST plasmas, in addition to KBMs, micro-tearing modes (MTM) were found unstable near the top of the pedestal [9, 11]. This suggests a model where the widening of the pedestal is due to MTMs in the shallow gradient region at the top of the pedestal becoming stabilised by increasing density and pressure gradients at the "knee" of the pedestal top, allowing the steep pressure gradient to increase until the KBM stability limit is reached [11].

Whilst the EPED model has been able to predict a large number of JET pedestal pressures at a 20-30% accuracy [12], some of the trends are not correctly predicted. In this paper we investigate the linear stability limit in the pedestal region of well-diagnosed ELM cycles in JET. The selected plasmas are from a density scan that shows mixed agreement with EPED predictions [13]. The pedestal width increases with $\beta_{p,ped}$ as predicted by the EPED model, but the scaling exponent cannot be determined accurately from the data. The EPED predicted pedestal pressure, however, shows a decreasing trend with increasing density while the opposite is observed experimentally: this discrepancy is discussed in more detail in [13].

We try to understand the underlying causes for the discrepancies by using linear ideal MHD and local gyrokinetic stability analyses. First in section 2, we construct the plasma equilibrium using the HELENA code [14] including the bootstrap current that is dominant in the edge region. HELENA also calculates the local $n = \infty$ ballooning stability for each flux surface. Then we use the HELENA equilibria to study the peeling-ballooning stability with a finite-n MHD stability code MISHKA-1 in section 3. Finally, the gyrokinetic code GS2 [15] is used to investigate the micro-stability in section 4. We determine the region that is locally unstable to KBMs during the ELM cycle and how well this corresponds to the region that is unstable to the ideal MHD $n = \infty$ ballooning modes. We will also investigate, whether unstable MTMs are found near the JET pedestal top.

2 Experiment and Equilibrium Reconstruction

2.1 Equilibrium Reconstruction Procedure

In order to study the MHD and gyrokinetic stability of the JET pedestal, we first need to accurately reconstruct the equilibrium. The electron density and temperature are obtained using the high resolution Thomson scattering diagnostics [16, 17]. The profiles are measured in R, Z coordinates, mapped to equilibrium poloidal flux by using the EFIT equilibrium, binned according to their timing in the ELM cycle and then the combined profiles are fitted with a *mtanh*-function [18] using a deconvolution technique described in [17]. Since the EFIT separatrix position is not very accurate, we adjust the radial position of the profiles so that the separatrix temperature matches with two-point power balance model[19]:

$$T_{e,sep}[eV] = \left(T_{div}^{\frac{7}{2}} + \frac{7}{2}(P_{heat} - P_{rad}) \frac{L_{||}}{\lambda_q 2\pi R_{OMP} k_0} \right)^{\frac{2}{7}} \quad (1)$$

where T_{div} is the temperature at the divertor (in eV), P_{heat} is the total heating power (in MW), P_{rad} is the total radiative power from the core (in MW), $L_{||} = \pi R_0 q_{95}$ is the parallel connection length (in m), λ_q is the radial power decay length (in m), R_{OMP} is the major radius of the outer midplane (in m) and k_0 is the heat conduction. The values used in this paper are either taken from the experiment $(R_0, P_{heat}, P_{rad}, q_{95}, R_{OMP})$ or assumed ($\lambda_q = 0.005$, $k_0 = 2000$).

For ion temperature, we have assumed that in the core $T_i = T_e$ and used two different assumptions for the pedestal, either $T_i = T_e$ or $dT_{i,ped}/d\psi = dT_{i,core}/d\psi$. It turns out that the choice of the assumption of ion temperature has little effect on the equilibrium and stability. For the Z_{eff}, which affects the bootstrap current through collisionality as well as ion density through dilution, we have used a line-integrated measurement and assumed constant value in the plasma. The line integrated Z_{eff} is taken from the visible Bremsstrahlung diagnostic.

The current profile is assumed to be a combination of inductively driven and bootstrap current. In the absence of edge current measurements we calculate the bootstrap current from density and temperature profiles using formulas in [20, 21]. We note that the bootstrap calculation in this paper

assumes constant $Z_{\rm eff}$ across the plasma, and that more recent improved calculations predict lower bootstrap current density at high collisionality [22]. In the stability analysis part we will conduct a scan in bootstrap current to evaluate the sensitivity of the stability results due to the variation in the bootstrap current. The inductively driven current is assumed to be fully relaxed to the neo-classical conductivity profile, which slightly overestimates the core current but has little effect on the equilibrium near the edge where the bootstrap current dominates. The plasma boundary shape is taken from EFIT. Using this information, we calculate a fixed boundary equilibrium that has a self-consistent bootstrap current with the HELENA code using the method described in [23].

To improve further the quality of the equilibrium, we redo the mapping of the profiles from real space into the flux space using the HELENA equilibrium. It turns out that the effect of this remapping on the profiles is small and the edge pressure gradient changes by less than 5%.

2.2 Investigated Plasmas

For this study, we have chosen two high triangularity ($\delta = 0.41$) ELMy H-mode JET discharges from a fuelling scan in the Carbon wall and divertor configuration with I_p=2.5 MA, B_t=2.7 T [13]. The discharges were selected from opposite ends of the fuelling scan (but at at sufficiently low density to avoid the transition to Type III ELMs), and with the highest available resolution of Thomson scattering data in the JET pedestal region. The discharge #79503 has high fuelling (2.6×10^{22}e/s) and the discharge #79498 has low fuelling (0.2×10^{22}e/s). The density, temperature and pressure profiles of the two plasmas during the ELM cycle are shown in Fig. 1. The period right after the ELM crash (0-10% of the ELM cycle) is ignored because the data in the period is dominated by the ELM crash and not very useful for analysis. Excluding it does not change any of the conclusions presented in the paper. A more detailed discussion about the data and fitting is given in [13]. $Z_{\rm eff}$ is 2.0 for the low fuelling case and 1.7 for the high fuelling case. While both plasmas have large Type I ELMs, the high fuelling case has also larger inter-ELM losses and the ELMs are classified as mixed Type I/Type II: we focus our analysis on the Type I ELM cycle in both plasmas.

As described in detail in [13], the pedestal behaviour between ELMs is different in these two cases. In the low fuelling plasma, both the temperature and density pedestal heights increase and the widths decrease during the

ELM cycle and the pressure gradient increases until the ELM crash collapses the pedestal. (Very similar profile evolution was observed in the two other low fuelling discharges with the highest available resolution of HRTS.) In the high fuelling case; the density pedestal height increases slightly while the temperature profile stays unchanged after the quick recovery following the ELM crash; initially (up to midway through the ELM cycle) the maximum pressure gradient in the pedestal increases, but then saturates and does not change for a large part of the ELM cycle. The width of the pressure profile increases very slightly during the ELM cycle. The time evolution of the pressure gradient and the pedestal width for both discharges are shown in Fig. 2. At the fully developed pedestal the ratios of the measured pedestal pressure height and width (in normalised poloidal flux) to the EPED1 predictions are: 0.94 and 0.83 respectively in the low fuelling discharge (#79498); and 1.38 and 1.35 respectively in the high fuelling discharge (#79503). The pedestal parameters in these particular discharges are entirely consistent with the trends over the fuelling scan that are illustrated in Figs. 16 and 17 of [13].

In the equilibrium reconstruction the self-consistent bootstrap current is assumed to follow the pressure profile without a delay. It has been shown that this is a good approximation for current diffusion in similar plasmas in ASDEX Upgrade [31]. The resulting toroidal current and q-profiles are shown in Fig.3. As can be seen, the q-profile develops a flat part in the location of the maximum bootstrap current.

3 MHD Stability analysis

3.1 Finite-n MHD Stability Analysis

The finite-n MHD peeling-ballooning instabilities have been found to limit the pedestal height in Type I ELMy H-mode plasmas in several devices [25]. In this paper, we use the MISHKA-1[26] ideal MHD code to investigate the finite-n stability of the plasma during the ELM cycle. We conduct two different types of scans around the experimental equilibrium. First we map the stability boundaries in $\alpha - < j_\phi >_{max}$-space. Here the normalized pressure gradient, α, is defined as [27]

$$\alpha = \frac{-2\partial V/\partial\psi}{(2\pi)^2}\left(\frac{V}{2\pi^2 R_0}\right)^{1/2}\mu_0\frac{\partial p}{\partial\psi}, \tag{2}$$

where V is the plasma volume, R_0 is the major radius and p is the pressure. $< j_\phi >_{max}$ is the maximum of the flux surface averaged toroidal current density in the pedestal region. In the scan we vary the $dp/d\psi$ and $< j_\phi >$ profiles from the experimental profile using the method described in detail in [30]. This method allows the profiles to be varied locally without introducing discontinuities.

The finite-n stability diagrams of the two discharges, for toroidal mode numbers in the range $3 < n < 30$, are shown in Fig. 4. In the diagrams the color represents the growth rate, γ, of the most unstable mode and the stability boundaries are drawn for $\gamma = 0$ and $\gamma = \omega_*/2$, where ω_* is half of the maximum diamagnetic frequency for a given mode number in the pedestal. The finite-n modes that become unstable late in the ELM cycle are peeling-ballooning modes with significant drive from the edge current density gradient $J'_\parallel$. Such peeling-ballooning modes are global in nature, have growth rates that peak at finite n and become stable as $n \to \infty$.

In both cases the edge plasma starts the ELM cycle deep in the stable region. In the low fuelling case the pressure gradient and the current density keep increasing until the end of the ELM cycle, when the plasma has crossed into the unstable region. Since the pedestal width of the last time point is close to the width of the instrument function used in the fitting, the deconvolution technique used in the fitting procedure may in this particular case overestimate the gradient that would explain the last time point being relatively deep in the unstable region. In the high fuelling case the pressure gradient and the current density saturate long before the ELM crash with the edge plasma close to marginal stability. As a conclusion of the finite-n stability analysis we can say that the result is consistent with the assumption in the EPED model that the peeling-ballooning modes are the ultimate limit for the pedestal height.

3.2 $n = \infty$ MHD Stability Analysis

It has been shown that $n = \infty$ MHD ballooning modes are unstable in the conditions of the MAST pedestal [9, 11], with stability boundaries that match closely those from local gyro-kinetic calculations of kinetic ballooning modes (KBMs).[2] In the analysis presented in [9] for the MAST plasma,

[2]Theoretically this is not surprising, as the kinetic result reduces to the MHD ballooning equation in the appropriate low frequency limit [10].

the edge plasma is relatively cold ($T_{e,ped} < 200$ eV) resulting in a relatively collisional plasma with a small bootstrap current peak. However, in the JET discharges analyzed in this paper the pedestal temperature is much higher ($T_{e,ped} \approx 1$ keV) and the resulting bootstrap current peak is large. As was shown in Fig. 3 the bootstrap current peak flattens the q-profile in the steepest pressure gradient region, locally stabilising ballooning modes. We investigate the $n = \infty$ ballooning stability by scaling the normalised pressure gradient α locally, checking the ballooning stability for each value of α and plotting the value of $F = \alpha_{crit}/\alpha_{exp}$, where α_{crit} is the marginally ballooning stable value of α and α_{exp} is the experimental value of α. Figure 5 shows the evolution of F during the ELM cycle in the two analyzed JET pedestals. In the graph, the flux surfaces where $F > 1$ are stable and those with $F < 1$ are unstable. As can be seen, there is a narrow band of unstable plasma between the steepest gradient and the edge. The steepest pressure gradient region is stable through the ELM cycle, as has been found previously in DIII-D and JET [24, 28, 29]. This local stability is due to the strong bootstrap current peak in the pedestal. The"knee" or the top of the pedestal is also stable, but closer to the stability limit than the steepest gradient region.

We demonstrate that the $n = \infty$ stability in the steepest pressure gradient region is due to the bootstrap current peak by conducting a scan in which we vary the amount of bootstrap current included in the equilibrium reconstruction. The results shown in Fig. 6 are from the equilibria at the end of the ELM cycle, but similar results are found for other time points. As can be seen more of the pedestal region indeed becomes unstable as the bootstrap current is reduced from the value given by the formulas in Ref. [20]. Without the large bootstrap current peak the entire steep pedestal region of the experimental equilibrium becomes unstable to $n = \infty$ ballooning modes. As can also be noted, the "knee" region becomes unstable with less reduction of current than is required to destabilize the steepest pressure region.

It is interesting to ask whether the surface with the steepest pressure gradient [3] and found to be locally ballooning stable due to the high bootstrap current, is unstable at an earlier time during the increase of the pressure pedestal. If ballooning instability arises earlier during the ELM recovery, KBMs might be expected to limit further local increases in pressure gradient. dP/dr may still, however, increase in ballooning stable regions of the pedestal, until possibly becoming clamped by KBMs over a broader region.

[3] Pressure gradients were obtained using *mtanh*-function fits.

This is the idea behind the ballooning critical pedestal (BCP) method used in the EPED 1.6 model [7]. If the steepest dP/dr surface remains locally ballooning stable throughout the ELM recovery, then the local analysis cannot predict any limit to the maximum dP/dr; if KBMs are also globally stable, dP/dr can grow until it becomes limited by another mechanism or by the ELM crash.

Fig. 5 demonstrated that the steepest pressure gradient regions of the JET pedestals are locally stable to $n = \infty$ ballooning modes throughout the ELM cycle. During the ELM cycle, however, both the width of the pedestal and the location of the steepest pressure gradient evolve. In order to study in isolation the effect of pedestal pressure profile steepening, we conduct an artificial equilibrium scan based on the profiles from the last point of the ELM cycle. In this scan we have varied the height of the temperature pedestal, obtained self-consistent equilibria with modified bootstrap current profiles, and tested $n = \infty$ ideal ballooning stability. The ideal $n = \infty$ ballooning unstable region is plotted as a function of $P_{\rm ped}$ in Fig. 7. We note that no unstable flux surfaces were found for pedestal pressure values lower than those shown in the plot. In both high and low fuelling plasmas the ballooning unstable region moves slightly inwards as $P_{\rm ped}$ is reduced, but the maximum dP/dr surface in the middle of the pedestal remains locally ballooning stable throughout both scans. At high fuelling the ballooning unstable region reaches into the outer part of the central-half of the pedestal at lower $P_{\rm ped}$, but at low fuelling the unstable region remains in a narrow region closer to the plasma edge. Only the very narrow outer region (especially in the case of the low fuelling plasma) appears to be limited by a local high n ballooning instability. We have also performed, over these $P_{\rm ped}$ scans for low and high fuelling plasmas, global ideal MHD stability analysis at high finite-n ($35 < n < 70$, extending the range of Sec. 3.1). These high n global modes were found to be stable throughout both scans. Fig. 4 shows that peeling-ballooning modes at lower n become unstable as $P_{\rm ped}$ approaches its pre-ELM value.

4 Gyro-kinetic analysis

Finite-n MHD stability of the plasma edge provides hard limits that cannot be breached without the loss of a considerable part of the plasma as happens during an ELM. However, more benign turbulence driven by local micro-

instabilities can also limit the edge gradients through transport. KBMs are micro-instabilities that trigger stiff transport above a critical pressure gradient, potentially limiting the pressure gradient to this critical value. Other types of mode may also be unstable in the pedestal, triggered by density or temperature gradients. Such modes also cause transport that affects the evolution of the pedestal, but do not directly limit the pressure gradient to a specific critical value.

To study the micro-instabilities in the pedestal region during the ELM cycle in more detail, we use local gyro-kinetic analysis, and we consider modes with size of the order of ion Larmor radius, which is generally small compared to the equilibrium scale lengths. At the top of the pedestal this requirement is easily met ($L_T/\rho_i \approx 80$ and $L_n/\rho_i \approx 800$), but in the steep gradient region the gyrokinetic expansion parameter is larger (both L_n/ρ_i and $L_T/\rho_i \approx 10-20$). We note that recent global gyro-kinetic analysis, agreeing with local flux-tube simulations at high n ($n > 21$), has demonstrated the existence of near-threshold conditions for kinetic ballooning modes in D-IIID H-mode pedestals [32].

4.1 Gyrokinetic stability in the steep gradient region

In the previous section we found that the JET plasmas are locally stable to $n = \infty$ ideal MHD ballooning modes across most of the pedestal, apart from in a narrow outer region. It is well known that ideal MHD ballooning modes and kinetic ballooning modes have very similar drive mechanisms [33]. Ideal MHD $n = \infty$ stability in the MAST pedestal has been found to be a reliable indicator of local kinetic ballooning mode (KBM) stability calculated by a local gyro-kinetic code [9]. We will now test if this is true also for the JET pedestal with higher bootstrap current. For this analysis we use the local electro-magnetic gyrokinetic code GS2 [15]. Both the ions and electrons are treated kinetically and the collisions are taken into account. The effect of sheared flow, while important for modes with growth rates similar to the shearing rate, may be less important for KBMs because once the plasmas crosses the stability boundary for KBMs, the growth rate increases very rapidly [8, 34] resulting only in a small increase in the critical pressure gradient. Therefore, the flow shear is neglected in this analysis. Future studies are planned to include the effect of the flow shear.

The linear local gyro-kinetic stability analysis at $k_\theta \rho_i$ <0.2 (k_θ is the poloidal wave number and ρ_i is the ion Larmor radius) finds no kinetic bal-

looning modes (KBM) in the JET pedestals. This agrees with the ideal MHD $n = \infty$ stability described earlier. At higher $k_\theta \rho_i$ ($0.2 < k_\theta \rho_i < 2$) we find ion temperature gradient/trapped electron modes (ITG/TEM) and at even higher $k_\theta \rho_i$ ($k_\theta \rho_i > 5$) electron temperature gradient (ETG) modes. These modes have growth rates that do not increase with β at constant R/L_p (where β is the ratio of plasma pressure to magnetic energy). ITG and ETG modes are not destabilized by increasing density gradient making them unlikely candidates for limiting the pedestal density gradient. Therefore, while it is possible that these modes play a role in the limiting of the pedestal temperature gradient and slowing down the pedestal recovery, in this paper we concentrate on KBMs that are destabilized by increasing pressure gradient and have very high growth rates producing stiff turbulent transport in all channels once the stability limit is exceeded [35].

We scan the plasma β locally in GS2 (without solving for a new self-consistent equilibrium using HELENA) to find the local stability limit for KBMs, which are found to be unstable at $k_\theta \rho_i \sim 0.1 - 0.2$ in these JET pedestals. The equilibrium scale length exceeds the corresponding rational surface spacing close to the pedestal top, but this local approximation is challenged in the steepest gradient region. As can be seen in Fig. 8, the amount by which β must be increased in order to destabilize KBMs matches very well with the F parameter in the $n = \infty$ ideal MHD analysis throughout the pedestal region. So, while the validity of the gyrokinetic theory in the pedestal region is marginal due to small L_n/ρ_i and L_T/ρ_i values, the local stability of KBMs still agrees very well with ideal MHD stability at $n = \infty$. We can also see that the regions closest to the stability limit are the bottom of the pedestal ($\psi \approx 0.99$) and the "knee" of the pedestal ($\psi \approx 0.94$ in high fuelling case and $\psi \approx 0.96$ in the low fuelling case). The steepest part of the pedestal is locally very stable to KBMs.

The reason for the good local stability to KBMs in the pedestal is the large bootstrap current that lowers the flux-surface averaged magnetic shear in the steep pressure gradient region. As was shown in the previous section, reducing the bootstrap current that is included in the equilibrium reconstruction destabilizes the local $n = \infty$ ballooning modes. Exactly the same happens with the KBMs in a local gyro-kinetic simulation. Figure 9 shows the local KBM growth rate in the pedestal region when no bootstrap current has been taken into account. In the low fuelling case, the local KBM growth rate has two peaks: one between the edge and the maximum pressure gradient and the other between the top of the pedestal and the maximum

pressure gradient. These peaks match very well with the ideal MHD $n = \infty$ ballooning unstable regions, i.e. the most $n = \infty$ ballooning unstable regions have also the highest local growth rates for KBMs. In the high fuelling case, the local KBM growth rate peaks just outside the steepest gradient region. Also in this case the region locally unstable to KBMs matches very well with the region unstable to ideal $n = \infty$ MHD ballooning modes.

4.2 Gyrokinetic stability at the pedestal top

In a gyro-kinetic analysis of the MAST tokamak, it was found that the plateau region at the top of the pedestal is unstable to micro-tearing modes (MTM) [36, 11, 37]. The identification of the micro-tearing modes in the JET pedestal top is made more difficult by other unstable micro-instabilities. In the JET pedestal top, ITG modes are the dominant instability. In order to identify possible sub-dominant micro-tearing modes, we make the equilibrium up-down symmetric and in GS2 suppress even parity modes such as the ITG. Changing the plasma shape to up-down symmetric has very little effect on the growth rates of the dominant mode. When the ITG modes are suppressed, we find sub-dominant odd parity micro-tearing modes. Figure 10 shows the growth rates of the ITG (unsuppressed case) and MTM (when ITG is suppressed) at the "knee" of the pedestal for both cases at the end of the ELM cycle. The growth rate spectra for different time points is qualitatively similar.

Similar to what was found in MAST [11, 36] and unlike micro-tearing modes found in the core, the mode structure of the pedestal top micro-tearing mode is not very extended along the field lines as shown in Fig. 11. We also find that this mode is relatively insensitive to the collisionality (growth rate increases slightly with decreasing collisionality) and is unstable even when collisions are dropped from the gyro-kinetic simulation. The growth rate of the MTM at the pedestal top decreases with increasing density gradient and increases with increasing temperature gradient as in [11, 36, 37]. MTMs can contribute to the transport of the pedestal top region, but would become suppressed by an increasing edge density gradient as described in [11].

5 Conclusions

This paper presents finite-n MHD stability analyses of carefully reconstructed

experimental pedestal equilibria from JET H-mode plasmas with Type I ELMs, with both high and low gas fuelling. At the end of the ELM cycle these pedestals are, within experimental uncertainties, limited by finite-n peeling-ballooning modes. This confirms previous results from JET and various other devices, and is consistent with the EPED model assumption that peeling-ballooning modes limit the pedestal. Earlier in the ELM cycle both plasmas are shown to be stable to finite-n peeling-ballooning modes over the range $3 < n < 30$. In the high fuelling case the pedestal saturates close to the peeling-ballooning stability boundary around half-way through the ELM cycle, while in the low fuelling case the pedestal pressure gradient keeps increasing until the ELM crash.

In the pedestal region, the stability boundaries obtained using local ideal MHD $n = \infty$ ballooning mode analysis and local linear gyro-kinetic analysis for kinetic ballooning modes show very good correspondence. This is consistent with MHD $n = \infty$ ballooning mode stability providing a reasonable indicator for the local stability of kinetic ballooning modes. Most of the pedestal region in these discharges is found to be locally stable to both modes, due to reduced magnetic shear caused by high bootstrap current in the steep pressure gradient region. The steepest pressure gradient surface of the pedestal remains locally stable throughout artificial scans about the pre-ELM equilibria, where the bootstrap current is computed self-consistently as the pedestal height is varied from a low value to its pre-ELM value. Furthermore, global MHD calculations find that all toroidal mode numbers in the range $35 < n < 70$ (i.e. at higher finite-n than peeling-ballooning modes) are stable throughout these scans.

We note that our local ballooning and finite-n peeling-ballooning stability results could be sensitive to any significant errors in the bootstrap current formula by Sauter *et al* [20] or in other equilibrium parameters. The sensitivity of local KBM stability to the bootstrap current density points to the need for accurate measurement of the edge current profile to validate the neoclassical models for the bootstrap current. Large bootstrap current density and low magnetic shear are expected in ITER pedestals, which may exclude KBMs from limiting the pedestal pressure gradient [38].

In the low fuelling JET plasma, the observation that the maximum pedestal pressure gradient increases over the ELM cycle, combines with the results from $n = \infty$ MHD and local gyro-kinetic analysis, to suggest that the maximum pedestal pressure gradient is not limited by kinetic ballooning modes during this ELM cycle. Furthermore, the narrowing of the pedestal through

this ELM cycle is very different to typical ELM cycles in DIII-D and MAST where the pedestal broadens with a constant maximum pressure gradient [39, 9].

These JET experiments were found to be consistent with the pedestal being ultimately limited by peeling-ballooning modes. The peeling-ballooning mode limit for the pedestal top pressure is relatively insensitive to the pedestal width [7, 38], and it may not be necessary to get the width exactly right in order to have a reasonable prediction for the pedestal height.

Gyro-kinetic analysis also found micro-tearing modes at the JET pedestal top with similar features to those found earlier in the MAST pedestal top [36, 37]. In these JET plasmas the peak growth rate of the microtearing modes is approximately half the peak growth rate of ITG modes. MTMs have been shown to be important, even when they are stable, in nonlinear electromagnetic simulations of ITG turbulence [40], and could play a role at the JET pedestal top where they are unstable but sub-dominant to ITG modes.

Our analysis finds that in these JET plasmas KBMs are locally stable in most of the pedestal (inboard of and including the maximum dP/dr surface) and locally unstable in a narrow region at the extreme edge. These local results suggest that KBMs have little impact on the evolution of most of the pedestal in these discharges, though we note that sheared flows and 3D equilibrium effects have not been included in this analysis. Gyrokinetic analysis has limitations in the pedestal when the ion Larmor radius approaches the equilibrium scale length, and the accuracy of local gyrokinetics is further restricted in the steep pedestal where the rational surface spacing approaches the equilibrium scale length. The latter limitation can be alleviated through global gyrokinetic calculations that include radial equilibrium variation. Our local analysis cannot exclude the possibility that a globally unstable KBM plays a role in the pedestal, but higher finite-n MHD ballooning mode calculations find no instability over the range $35 < n < 70$. Investigation of this possibility requires a global gyrokinetic calculation, which will be considered in future work.

Acknowledgements

The authors are grateful to Jack Connor, Jim Hastie, Phil Snyder and Howard Wilson for several stimulating discussions. This work was partly funded by

the RCUK Energy Programme under grant EP/I501045 and the European Communities under the contract of Association between EURATOM and CCFE and carried out within the framework of the European Fusion Development Agreement. The views and opinions expressed herein do not necessarily reflect those of the European Commission. The gyrokinetic calculations were carried out on HECToR supercomputer (EPSRC grant EP/H002081/1).

References

References

[1] Ryter F. et al., Plasma Phys. Control. Fusion **43** (2001) A323

[2] Saarelma S. et al., Plasma Phys. Control. Fusion **51** (2009) 035001

[3] Snyder P.B., et al. Nucl. Fusion **44** (2004) 320

[4] Saibene G., et al., Nucl. Fusion **47** (2007) 969

[5] Snyder P.B. et al., Phys. Plasmas **16** (2009) 056118

[6] Beurskens M.N.A. et al., Phys. Plasmas **18** (2011) 056120

[7] Snyder P.B. et al., Nucl. Fusion **51** (2011) 103016

[8] Snyder P.B. and G.W. Hammett, Phys. Plasmas **8** (2001) 744

[9] Dickinson D. et al., Plasma Phys. Contr. Fusion **53** (2011) 115010

[10] W.M. Tang, J.W. Connor and R.J. Hastie, Nucl. Fusion **20**, 1439 (1980)

[11] Dickinson D. et al., Phys. Rev. Lett. **108**,

[12] Beurskens M.N.A. et al., Nucl. Fusion **53**, 013001 (2013)

[13] Leyland M.J. et al., Nucl. Fusion **53** (2013) 083028

[14] Huysmans G.T.A., Goedbloed J.P., Kerner W.O.K., Computational Physics (Proc. Int. Conf. Amsterdam, 1991),World Scientific Publishing, Singapore (1991) 371

[15] Kotschenreuther M., et al., Comput. Phys. Commun **88** (1995) 128

[16] Pasqualotto R. et al., Rev. Sci. Instrum. **75**, (2004) 3891

[17] Frassinetti L., et al., Review of Sci. Instr., **83** (2012) 013506

[18] Groebner R. J. et al., Plasma Phys. Contr. Fusion **44**, (2002) A265

[19] Kallenbach A., et al., J. of Nucl. Mater. **337-339**, (2005) 381

[20] Sauter O., Angioni C., Lin-Liu Y.R., Phys. Plasmas, **6** (1999) 2834

[21] Sauter O., Angioni C., Lin-Liu Y.R., Phys. Plasmas, **9** (2002) 5140

[22] Koh S. et al., Phys. Plasmas **19** (2012) 072505

[23] Saarelma S. et al., Plasma Phys. Contr. Fusion **51** (2009) 035001

[24] Miller R.L. et al., Plasma Phys. Control. Fusion **40** (1998) 753

[25] Snyder P.B. et al., Nucl. Fusion **49** (2009) 085035

[26] Mikhailovskii A.B. et al., Plasma Phys. Rep. **23** (1997) 844

[27] Miller R.L., et al., Phys. Plasmas **5** (1998) 973

[28] Lao L.L. et al., Nucl. Fusion **39** (1999) 1785

[29] Lönnroth J-S et al., Plasma Phys. Control. Fusion **46** (2004) 767 (2012) 135002

[30] Saarelma S. et al., Nucl. Fusion **52** (2012) 103020

[31] Burckhart A., et al., Plasma Phys. Contr. Fusion **52** (2010) 105010

[32] Wan W. et al., Phys. Rev. Lett. **109** (2012) 185004

[33] Kotschenreuther M., Phys Fluids **29** (1986) 2898

[34] Roach C.M. et al., Plasma Phys. Control. Fusion **47** (2005) B323

[35] Rewoldt G. et al., Phys. Fluids **30** (1987) 807

[36] Dickinson D. et al., to appear in Plasma Phys. Control. Fusion (2013), http://arxiv.org/abs/1209.3695

[37] Roach C.M. et al., Proceedings of 24th IAEA Fusion Energy Conference, TH/5-1, (2012), http://www-naweb.iaea.org/napc/physics/FEC/FEC2012/papers/176_TH51.pdf, in preparation for submission to Nucl. Fusion.

[38] Saarelma S. et al., Nucl. Fusion **52** (2012) 103020

[39] Groebner R.J. et al., Nucl. Fusion **50** (2010) 064002

[40] Hatch D.R. et al, Phys. Rev. Lett. 108, 235002 (2012)

List of Figures

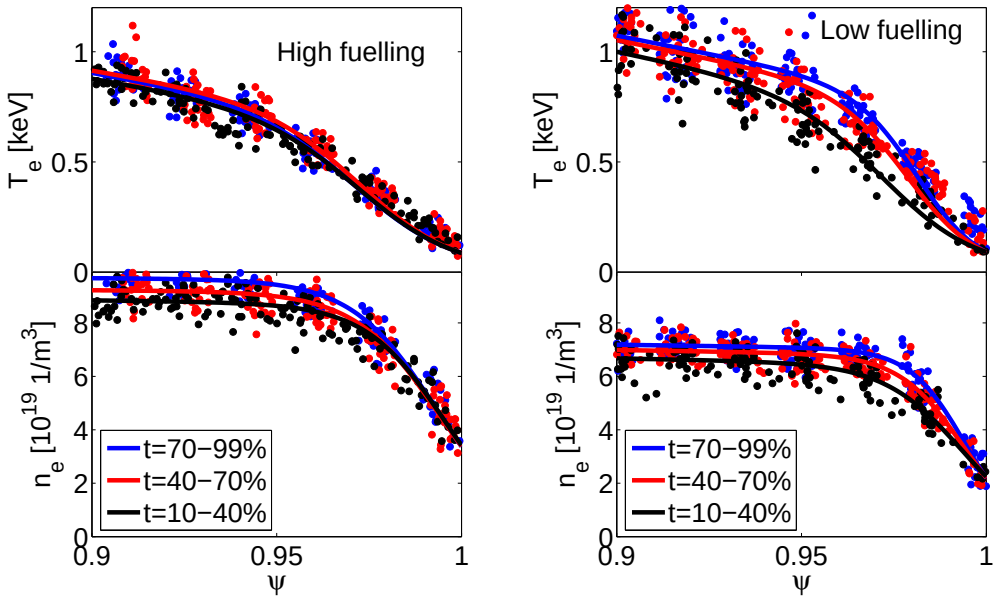

Figure 1: The density and temperature profile evolution during the ELM cycle in high (left) and low (right) fuelling JET discharges. The labels represent the normalized time in the ELM cycle.

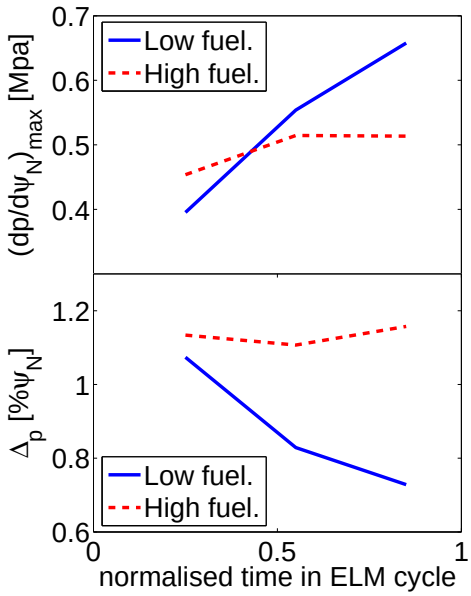

Figure 2: The time evolution of the maximum of the pedestal pressure gradient and the pedestal width during the ELM cycle in the high and low fuelling JET discharges.

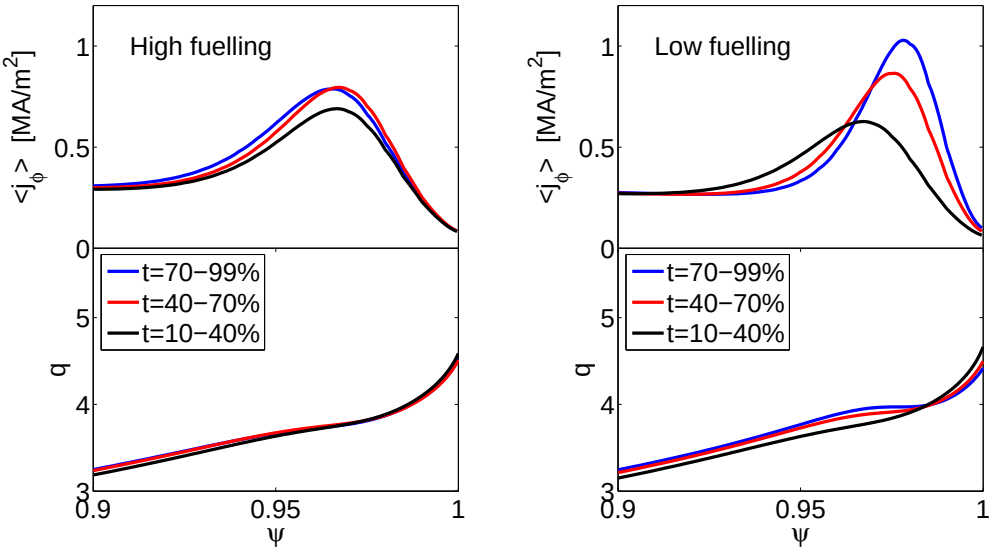

Figure 3: The flux surface averaged toroidal current and q- profile evolution during the ELM cycle in high (left) and low (right) fuelling JET discharges. The labels represent the normalized time in the ELM cycle.

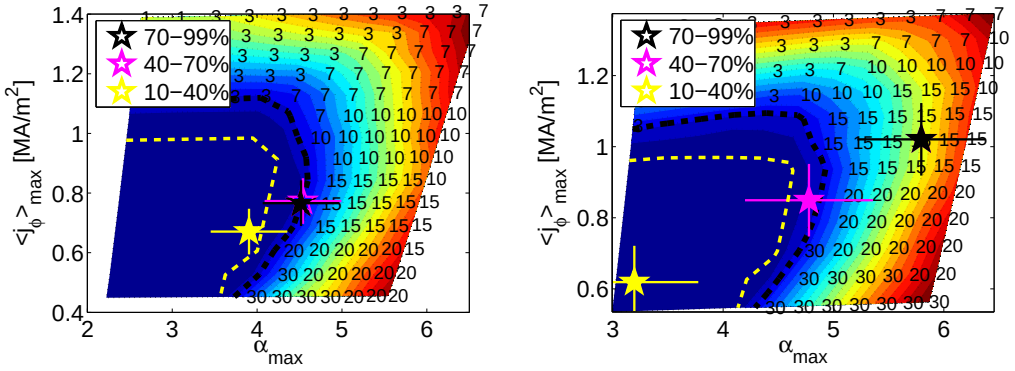

Figure 4: The peeling-ballooning mode stability diagrams, for toroidal mode numbers in the range $3 < n < 30$, for the high fuelling (left) and low fuelling (right) plasmas during the ELM cycle. The color represents the growth rate of the fastest growing mode (red is stable) and the numbers give the toroidal mode number of the most unstable mode. The dashed lines shows the stability limit at $\gamma > \omega * /2$ (black) and $\gamma > 0$ (yellow). The stars with the cross show the position of the experimental equilibrium during the ELM cycle and their estimated errors [13].

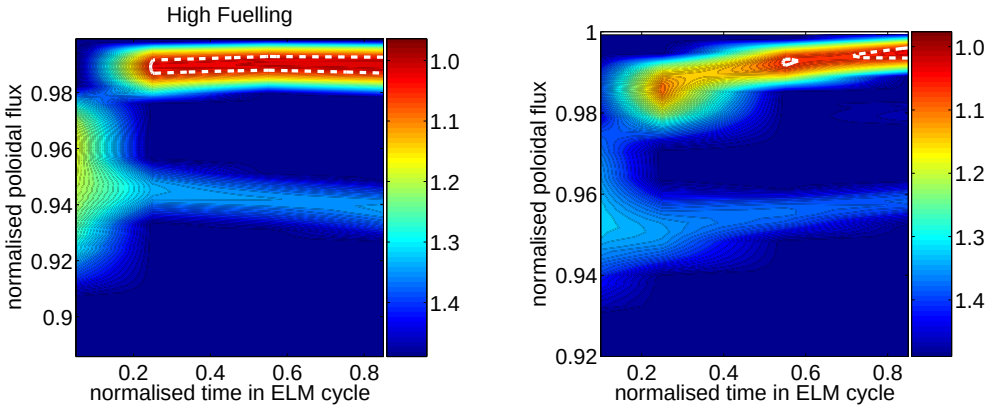

Figure 5: The $n = \infty$ ballooning stability during the ELM cycle in the edge region for the high (left) and low (right) fuelling cases. The colors represent the value of $F = \alpha_{crit}/\alpha$, where α_{crit} is the marginally ballooning stable value of α, i.e. regions below unity are unstable and above unity stable. The dashed line shows the region of marginal stability.

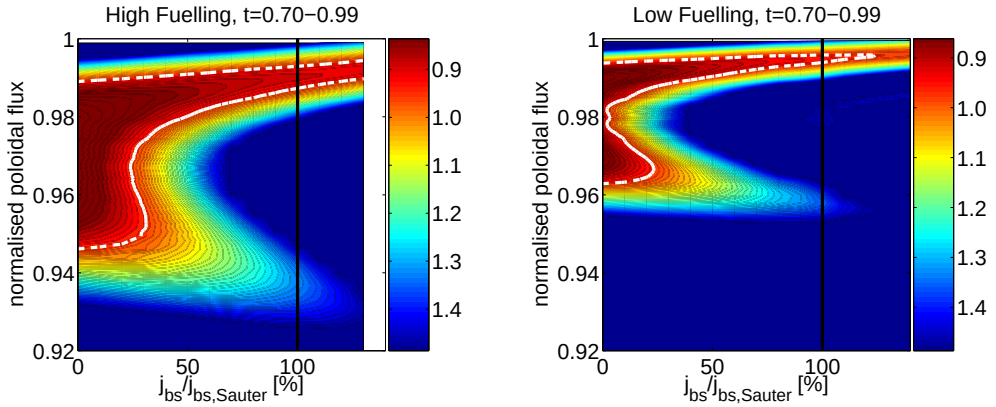

Figure 6: The $n = \infty$ ballooning stability as a function of bootstrap current taken into account in the equilibrium reconstruction for the pedestal region of high (left) and low (right) fuelling case at the end of the ELM cycle. The colors represent the stability (blue unstable, red stable) and the dashed white line shows the boundary of marginal stability. The vertical line represents the equilibrium with full bootstrap current given by the formula [20].

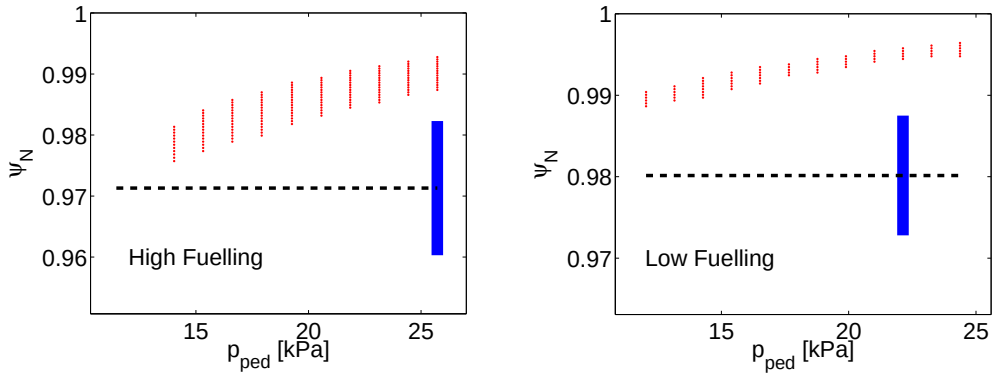

Figure 7: The $n = \infty$ ballooning unstable region in high (left) and low fuelling (right) cases when the pedestal top temperature is varied self-consistently. The red dots show the ballooning unstable flux surfaces. The blue line represents the region of the pressure pedestal from 25% to 75% of the height and is placed at the value of the experimental pedestal height. The black dashed line shows the steepest gradient location.

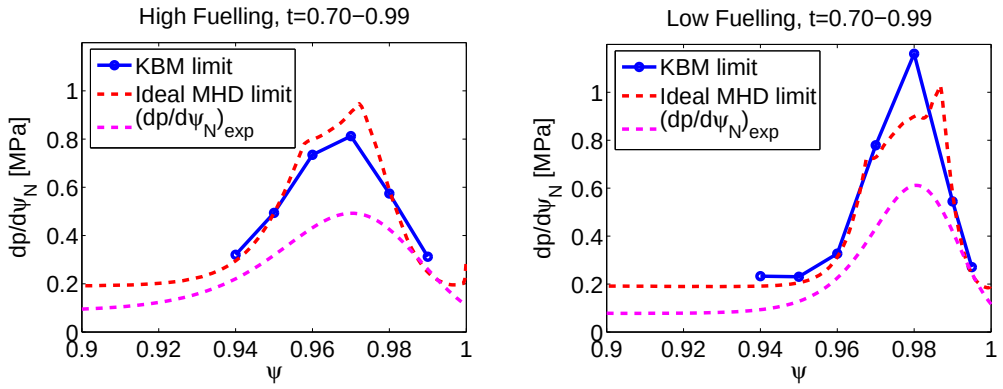

Figure 8: The gyro-kinetic stability limit of KBMs (solid blue line) in high (left) and low (right) fuelling pedestals at the end of the ELM cycle as a function of poloidal flux. For comparison, the $n = \infty$ ideal MHD ballooning stability limit (dashed red line) and the experimental pressure gradient (dotted magenta line) are also shown. The stability limits represent the value the pressure gradient can be increased before becoming unstable

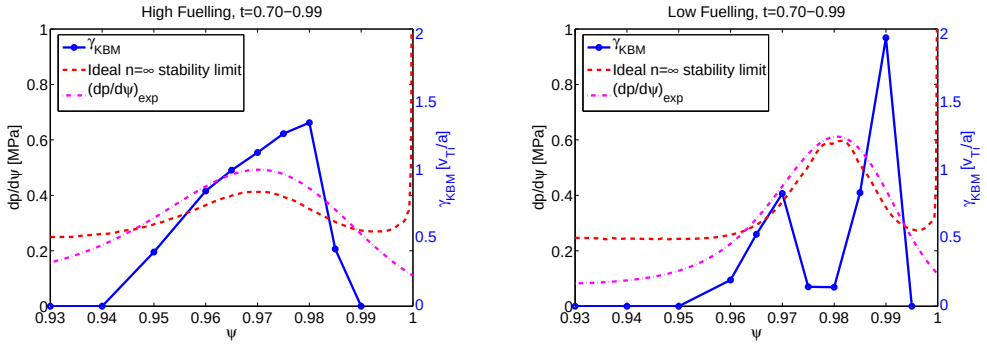

Figure 9: The growth rate of the kinetic ballooning mode (solid blue line, y-axis on the right) at the end of the ELM cycle in the edge region of high (left) and low (right) fuelling case with no bootstrap current used in the equilibrium reconstruction. Also shown is the $n = \infty$ ballooning stability limit (dashed red line, y-axis on the left) and the normalized pressure gradient (dash-dot magenta line, y-axis on the left).

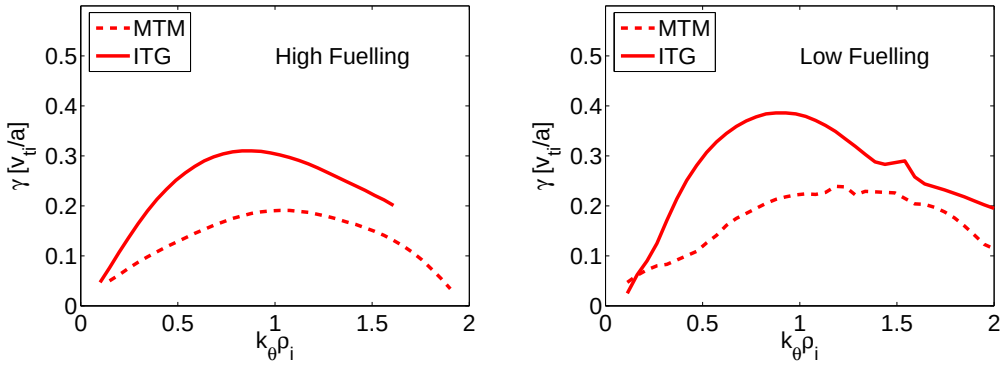

Figure 10: The growth rate spectrum of MTM and ITG modes in high (left) and low (right) fuelling case at the pedestal "knee" at the end of the ELM cycle. The ITG growth rates are calculated without restrictions for growing modes, while the MTM growth rates are obtained by suppressing all even parity modes.

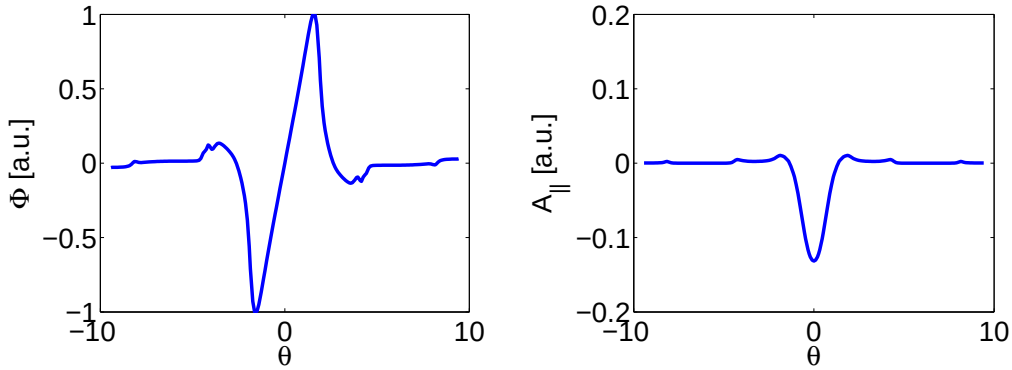

Figure 11: The eigenfunctions of electrostatic potential ϕ and parallel magnetic vector potential $A_{||}$ along the ballooning angle θ for the $k_y\rho_i = 0.37$ micro-tearing mode at the JET pedestal top.